



# The Efficacy of MRI in the diagnostic workup of cystic fibrosis-associated liver disease: A clinical observational cohort study

Sarah Poetter-Lang<sup>1</sup> · Katharina Stauffer<sup>2</sup> · Pascal Baltzer<sup>1</sup> · Dietmar Tamandl<sup>1</sup> · Dina Muin<sup>1</sup> · Nina Bastati<sup>1</sup> · Emina Halilbasic<sup>2</sup> · Jacqueline C. Hodge<sup>1</sup> · Michael Trauner<sup>2</sup> · Lili Kazemi-Shirazi<sup>2</sup> · Ahmed Ba-Ssalamah<sup>1</sup>

Received: 26 December 2017 / Revised: 27 June 2018 / Accepted: 3 July 2018 / Published online: 27 July 2018  
© The Author(s) 2018

## Abstract

**Purpose** To identify independent imaging features and establish a diagnostic algorithm for diagnosis of cystic fibrosis (CF)-associated liver disease (CFLD) in CF patients compared to controls using gadoxetic acid-enhanced MRI.

**Methods** A total of 90 adult patients were enrolled: 50 with CF, 40 controls. The CF group was composed of two subgroups: a retrospective test subgroup (n = 33) and a prospective validation subgroup (n = 17). Controls (patients with normal liver enzymes and only benign focal liver lesions) were divided accordingly (27:13). MRI variables, including quantitative and qualitative parameters, were used to distinguish CFLD from controls using clinical symptoms, laboratory tests and Debray criteria. Disease severity was classified according to Child-Pugh and Albumin-Bilirubin (ALBI) scores. Fifteen qualitative single-lesion CF descriptors were defined. Two readers independently evaluated the images. Univariate statistical analysis was performed to obtain significant imaging features that differentiate CF patients from controls. Through multivariate analysis using chi-squared automatic interaction detector (CHAID) methodology the most important descriptors were identified. Diagnostic performance was assessed by receiver-operating characteristic (ROC) analysis.

**Results** Three independent imaging descriptors distinguished CFLD from controls: (1) presence of altered gallbladder morphology; (2) periportal tracking; and (3) periportal fat deposition. Prospective validation of the classification algorithm demonstrated a sensitivity of 94.1% and specificity of 84.6% for discriminating CFLD from controls. Disease severity was well associated with the imaging features.

**Conclusions** A short unenhanced MRI protocol can identify the three cardinal imaging features of CFLD. The hepatobiliary phase of gadoxetic acid-enhanced MRI can define CFLD progression.

## Key Points

- Using a multivariate classification analysis, we identified three independent imaging features, altered gallbladder morphology (GBAM), periportal tracking (PPT) and periportal fat deposition (PPFD), that could diagnose CFLD with high sensitivity, 94.1 % (95% CI: 71.3–99.9) and moderate specificity, 84.6 % (95% CI: 54.6–98.1).
- Based upon the results of this study, gadoxetic acid-enhanced MRI with DWI is able to diagnose early-stage CFLD, as well as its progression.

**Keywords** Cystic fibrosis · Magnetic resonance imaging · Chemical shift imaging · Gallbladder · Liver diseases

✉ Ahmed Ba-Ssalamah  
ahmed.ba-ssalamah@meduniwien.ac.at

<sup>1</sup> General Hospital of Vienna (AKH), Department of Biomedical Imaging and Image-guided Therapy, Medical University Vienna, Waehringer Guertel 18-20, A-1090 Vienna, Austria

<sup>2</sup> Division of Gastroenterology and Hepatology, Department of Internal Medicine III, General Hospital of Vienna (AKH), Medical University of Vienna, Vienna, Austria

## Abbreviations

3-T	3-Tesla
ALBI	Albumin-bilirubin score
ALT	Alanine aminotransferase
ALP	Alkaline phosphatase
AP	Antero-posterior
AST	Aspartate aminotransferase
BDA	Bile duct abnormalities
CC	Craniocaudal
CF	Cystic fibrosis

CFLD	Cystic fibrosis-associated liver disease
CFTR	Cystic fibrosis transmembrane conductance regulator
CHAID	Chi-squared automatic interaction detector
CM	Contrast media
CPS	Child-Pugh score
CSI	Chemical shift imaging
CT	Computed tomography
DWI	Diffusion-weighted imaging
GBAM	Altered gallbladder morphology
Gd-EOB-DTPA	Gadolinium ethoxybenzyl diethylenetriaminepentaacetic acid
GGT	Gamma-glutamyltransferase
HBP	Hepatobiliary phase
LL	Latero-lateral
MRCP	Magnetic resonance cholangiopancreatography
MRI	Magnetic resonance imaging
NPV	Negative predictive value
PACS	Picture Archiving and Communication System
PPF	Periportal fibrosis
PPFD	Periportal fat deposition
PPT	Periportal tracking
PPV	Positive predictive value
PSC	Primary sclerosing cholangitis
pv	Portal venous
RLE	Relative liver enhancement
RNH	Regenerative nodular hyperplasia
ROC	Receiver-operating characteristic
SI	Signal intensity
UDCA	Ursodeoxycholic acid
US	Ultrasound

## Introduction

Cystic fibrosis (CF) is one of the most common, lethal, autosomal recessive diseases of the Caucasian population. CF may affect any mucous-dependent organ, primarily the respiratory and digestive tracts [1]. So-called cystic fibrosis-associated liver disease (CFLD) may progress to end-stage liver cirrhosis, requiring curative liver transplantation [2]. CFLD, one of the cholestatic liver diseases, has been observed in up to 35% of CF patients during long-term follow-up [3]. Due to lung transplantation and optimised medical care, the survival of CF patients has improved [4, 5], such that CFLD is now considered the third leading cause of death, after primary lung disease and post-transplantation complications [6]. Therefore, early diagnosis of CFLD is crucial as some centres may initiate UDCA treatment as early as possible to improve liver function [7]. Unfortunately, both clinical and biochemical findings have

low sensitivity and specificity for CFLD [8]. Likewise, data on the features of early-stage CFLD are still in rudimentary development. Ultrasound (US) or computed tomography (CT) can depict only the morphologic features of CFLD at very advanced stages [9]. Conventional magnetic resonance imaging (MRI), including MR cholangiopancreatography (MRCP), is useful for assessing the hepatobiliary complications of CF. In previous studies, a wide range of hepatobiliary manifestations from hepatomegaly and diffuse fatty liver infiltration to severe cirrhosis with portal hypertension have been described [10]. Furthermore, biliary manifestations including strictures of intra- and extrahepatic bile ducts [11], as well as altered gallbladder morphology, such as cholelithiasis, sludge, micro- and macro-gallbladder have also been reported [9]. More recently, MRI techniques have been introduced, such as diffusion-weighted imaging (DWI) and hepatobiliary gadoteric acid-enhanced MRI, which are increasingly used in hepatobiliary imaging [12]. Gadoteric acid-enhanced MRI detects focal liver lesions and also provides information about regional and global function of the hepatobiliary system [13]. DWI, because of its inherent ability to detect subtle changes in hepatobiliary tissue [14], would be expected to detect CFLD at very early stages.

Our study aim was to identify independent imaging features and establish a diagnostic algorithm for the diagnosis of CFLD as compared with a control group using gadoteric acid-enhanced MRI.

## Patients and methods

The ethics review board of our institution approved the prospective and retrospective data collection and analysis. However, informed consent was obtained only from the prospective group patients. The requirement for informed consent was waived for the retrospective group. The study cohort was determined from our institutional database as shown in the flow chart (Fig. 1).

A total of 90 adult patients were included, 50 with CF and 40 controls who were examined using identical parameters. From October 2011 to November 2013 we retrospectively enrolled 33 consecutive patients with CF, at any stage. We then gathered 27 consecutively liver-healthy controls who had an MRI for the diagnostic work-up of benign focal liver lesions. The controls had no further hepatobiliary abnormalities or elevated liver enzymes. These 60 patients from the retrospective CF group and controls were used as a training cohort.

From February 2014 to March 2015, we enrolled another 17 CF patients and 13 consecutive liver-healthy controls prospectively to validate the classification algorithm established with the training cohort. All control patients were gathered between March 2010 and December 2014. The retrospective and prospective CF groups were

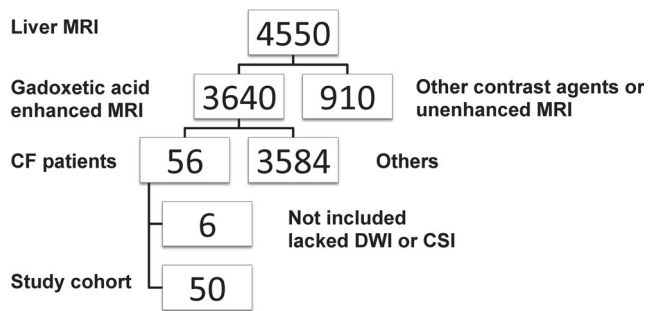


**Fig. 1** Flowchart: between 2011 and 2015, 3,640 patients underwent a standardized 3.0-Tesla gadoteric acid-enhanced MRI of the liver. Fifty-six patients with cystic fibrosis (CF) were enrolled. Due to lack of diffusion-weighted imaging (DWI) or chemical shift imaging (CSI) we excluded six patients. Therefore, the final study cohort consisted of 50 patients

selected by the hepatologists after excluding other liver diseases.

They were sent to MRI due to inconclusive ultrasound screening. In all patients an identical gadoteric acid-enhanced MRI protocol with DWI was applied. CFLD was defined by our hepatologists according to clinical symptoms, laboratory tests and Debray criteria [15].

In all patients, diagnosis of CF was definitively confirmed by our hepatologists. CF was diagnosed according to international criteria [16]. In addition, the majority of study patients had already had a double lung transplant for CF-associated lung disease at the time of study inclusion.

To estimate the severity of liver disease we used the Child-Pugh Score (CPS) for patients with cirrhosis [17], and the Albumin-Bilirubin (ALBI) score [18] for all patients.

Liver function tests, including serum bilirubin level, alkaline phosphatase (ALP), gamma-glutamyltransferase (GGT), aspartate aminotransferase (AST), alanine aminotransferase (ALT) and thrombocytes, were evaluated within 3 months of the MRI investigations. Clinical data for CF and controls were documented.

## MRI examination protocol

All MRI examinations were performed on a single 3-T MRI system (Magnetom TrioTim, Siemens Medical Systems, Erlangen, Germany). The MR imaging protocol is depicted on Table 1.

All patients received a bolus injection of 0.025 mmol/kg/body weight gadoteric acid (gadolinium ethoxybenzyl diethylenetriaminepentaacetic acid, Gd-EOB-DTPA, Primovist® Bayer) into a cubital or antecubital vein at 1 ml/s, followed by a 20-ml saline flush using a power injector.

## Image analysis

All MR images were reviewed on a commercial PACS system independently by two observers. Two radiologists, one with

more than 20 years of experience in abdominal MR imaging (AB), the other in the sixth training year (SP), randomly evaluated the retrospective and prospective CF and control group patient images. Both observers were blinded to the subgroup, the pathological diagnosis and the clinical data. For training purposes, the readers jointly reviewed 20 sample MRI cases of patients with CF (n=10) and control patients (n=10) who were not included in this cohort study. The inter-observer variability was calculated.

Quantitative and qualitative assessment was performed.

## Quantitative assessment

Liver and spleen volumes were calculated by measuring the maximum dimension of the liver and spleen in three perpendicular axes: craniocaudal (CC), latero-lateral (LL) and antero-posterior (AP) [19]. In addition, the portal vein diameter was measured for each patient and a diameter above 12 mm was defined as abnormal [20].

The signal intensity (SI) in the left liver lobe, and in liver segments VI, VII and VIII were obtained and the relative liver enhancement (RLE) was calculated by measuring the SI in the left liver lobe and in segments VI, VII and VIII in unenhanced T1-weighted images, as well as the T1-weighted images, 20 min after the administration of gadoteric acid in the HBP using the following formula:

$$\text{RLE (\%)} = \frac{\text{HBP enhanced SI}_{\text{liver}} - \text{unenhanced SI}_{\text{liver}}}{\text{unenhanced SI}_{\text{liver}}}$$

Furthermore, the SI of the spleen on in- and opposed-phase images was measured to calculate the corrected chemical shift imaging (CSI) hepatic fat fraction [21].

CSI<sub>hepatic fat fraction spleen correction</sub>

$$= \frac{(\text{SI}_{\text{in phase liver}}/\text{SI}_{\text{spleen}}) - (\text{SI}_{\text{opposed phase liver}}/\text{SI}_{\text{spleen}})}{2 \times \text{SI}_{\text{in phase liver}}/\text{SI}_{\text{spleen}}}$$

All quantitative assessments were performed by both readers in consensus.

## Qualitative assessment

For the qualitative assessment, we scored the presence or absence of distinct qualitative MRI features, some taken from the literature [22, 23], as well as those from our longstanding clinical experience in MRI liver imaging.

A total of 15 qualitative features representing diffuse and focal liver changes on distinct MR-sequences were rated as present =1 or absent =0, including: 1 – diffuse steatosis, 2 – periportal fat deposition (PPFD) (a linear periportal SI decrease on opposed-phase compared to in- phase), 3 –

**Table 1** MR protocol and examination parameters

Sequence	Section thickness (mm)	TR (ms)	TE (ms)	FOV (mm)	Phase direction	Flip angle	Acquisition time
GRE-T1 (flash 2D) in-phase	5	130	2.46	350	AP	70	2 × 17 s
GRE-T1 (flash 2D) opposed-phase	5	131	3.69	350	AP	70	2×17 s
T1 VIBE SPAIR axial, unenhanced, arterial, PV, transitional and hepatobiliary phases	1.7	2.67	0.97	430	AP	13	20 s
T1 VIBE SPAIR coronal PV phase and hepatobiliary phase	2	2.6	0.92	500	RL	13	20 s
T2 Haste coronal	4.5	805	76	450	RL	141	3×20 s
DWI axial TSE-EP	6	1700	73	380	AP	---	Resp. trigg. 4min.
T2 SE axial fs	5	2000	95	370	AP	165	Resp. trigg. 4 min
T2 Haste axial fs	5	1800	150	400	AP	150	3x20 s

2D two-dimensional, AP antero-posterior, DWI diffusion-weighted imaging, FOV field of view, fs fatsat, GRE gradient echo, RL right to left, SPAIR spectral-attenuated inversion recovery, TE echo time, TR repetition time, TSE turbo spin echo, VIBE volumetric interpolated breath-hold examination

periportal tracking (PPT) on DWI (a linear periportal increase in signal intensity), 4/5 – bile duct abnormalities (BDA) on T2-weighted/MRCP images and T1-weighted post-contrast images (irregularities of either stenosis or segmental dilatation or both), 6 /7 – heterogeneous liver parenchyma on DWI or and T1-weighted post contrast images, 8 – the degree of hepatobiliary uptake (this was evaluated both quantitatively by measuring the relative liver enhancement and qualitatively by visual impression in comparison to the kidney – brighter, equal or less bright), 9 – timely hepatobiliary excretion (presence of the contrast media in the common bile duct or even in the duodenum within 20 min after administration of contrast media (CM) was defined as timely excretion), 10 – altered gallbladder morphology (GBAM) (this includes micro-, macro-gallbladder, sludge and/or the presence of stones), 11 – periportal fibrosis (PPF) (means linear periportal decrease in signal intensity on DWI), 12 – the presence of regenerative nodular hyperplasia (RNH), 13 – widening of the fissures and hilum [24], 14 – portal vein dilatation (the portal vein diameter was measured on the pv post-contrast images), and 15 – the presence of lymph nodes in the hepatoduodenal ligament.

### Statistical analysis

Statistical analysis was performed using the IBM SPSS version 22.0 and the MedCalc statistical software version 15.4 for Windows.

Descriptive statistics were calculated to describe the study sample and were expressed as mean, range and absolute numbers. Categorical univariate variables (15 single-feature descriptors) were expressed as count and proportions and analysed using univariate Chi-square and Fisher's exact tests.

Count variables were analysed and compared between groups using non-parametric Whitney-Mann-U tests.

Levels of interobserver agreement were assessed using Cohen's kappa statistics, as defined in a study by Landis and Koch. Significant variables ( $p < 0.05$ ) at univariate analysis were used as input variables for Bonferroni-corrected, ten-fold, cross-validated multivariate classification analysis (Chi-squared Automated Interaction Detection Algorithm - CHAID) [25]. The minimal case number for parent nodes was set to ten, for child nodes to five. All CHAID analyses were performed using standard proprietary SPSS procedures.

First, the results of the retrospective cohort were obtained and then tested for the prospective cohort. The diagnostic accuracy of the classification tree was evaluated by receiver-operating characteristics (ROC) curve (AUC) analysis with 95% confidence intervals (Cis) using Medcalc.

## Results

### Demographic data

A total of 90 adult patients were enrolled, 50 with CF and 40 without liver disease (controls). The retrospective (test) CF subgroup ( $n = 33$ , mean age  $30.3 \pm 9.7$  years) consisted of 15 male and 18 female patients. The prospective (validation) group ( $n = 17$ , mean age  $35.8 \pm 11.2$  years) consisted of nine male and eight female patients (Table 2).

### Clinical and laboratory parameters

Comparing the two CF subgroups to the controls, only the cholestatic parameters, i.e. ALP and GGT, were significantly

**Table 2** Patient characteristics and laboratory tests

	CF Retrospective group	CF Prospective group	Controls 1	Controls 2	<i>p</i> -value Retrospective group vs. controls 1	<i>p</i> -value Prospective group vs. controls 2
Patient number	33	17	27	13	n.s.	n.s.
Males	15	10	10	8	n.s.	n.s.
Females	18	7	17	5	n.s.	n.s.
Mean age (y)	30.3 ± 9.7	35.8 ± 11.2	51.2 ± 16.9	48.9 ± 13.9	<0.001	<0.001
Serum bilirubin (<1.2 mg/dl)	0.89±1.6	0.51±0.25	0.74±0.57	0.71±0.66	0.60	0.84
AP (35–105 U/L)	135.7±138.4	106.8±64.3	63.0±17.2	58.47±13.45	<0.05	<0.05
GGT (<40 U/L)	82.1±128.1	52.4±96.6	32.4±28.3	33.73±33.66	<0.05	<0.05
AST (<35 U/L)	39.2±61.4	30.5±16.6	30.3±31.5	33.95±39.17	0.47	0.52
ALT (<35 U/L)	41.8±50.9	37.9±35.0	26.7±15.4	27.57±17.14	0.11	0.07
Serum Albumin (35–52 g/L)	38.42±10.5	35.3±13.3	41.8±6.9	43.8±3.8	0.15	0.18

Data are presented as means ± standard deviations Laboratory tests: alkaline phosphatase (AP), gamma-glutamyltransferase (GGT), aspartate aminotransferase (AST), alanine aminotransferase (ALT) *p*-values are based upon Whitney-Mann-U tests *n.s.* not significant

higher in the CF groups ( $p < 0.05$ ; CF vs. controls). The remaining liver function parameters were not significantly different between the two groups (Table 2).

From the 50 CF patients only eight patients showed liver cirrhosis according to the Child-Pugh score. There were three CPS A and three CPS B in the retrospective CF group and two CPS A in the prospective CF group. The remaining patients had no clinical evidence of liver cirrhosis. In the retrospective CF group, 25 patients were ALBI 1 and eight patients ALBI 2. In the prospective CF group, 13 patients had an ALBI 1 score, and four patients had an ALBI 2 score (Table 3).

## Imaging parameters

### Quantitative features univariate analysis

Our results showed that splenic volume was significantly higher in the two CF subgroups, as compared to the controls ( $p < 0.05$ ). The portal vein diameter ( $p = 0.43$ ) and liver volume ( $p = 0.18$ ) did not differ significantly. Likewise, the degree of

hepatic steatosis ( $p = 0.90$ ) and the RLE ( $p = 0.91$ ) were not significantly different in either CF group compared to the controls (Table 4).

The MR imaging features of cirrhosis including periportal fibrosis, irregular liver margins and bile duct abnormalities in the hepatobiliary phase associated well with CPS. The CM-uptake as a functional parameter associated significantly with the ALBI score, which, again, was indicative of advanced liver disease (Table 3).

### Qualitative features univariate analysis

As there was a very high inter-reader agreement using Cohen's kappa ( $\kappa = 0.8$ ), the qualitative assessment of the MR images of the more experienced reader was taken for further analysis. These showed significantly more patients with several distinct MR features in both the retrospective and prospective CF groups compared to the controls  $p < 0.001$  (Table 5), but there were no essential differences between the CF subgroups  $p > 0.05$ .

**Table 3** Association between severity of liver disease and Albumin-bilirubin (ALBI) score and Child-Pugh score (CPS) in the retrospective and prospective cystic fibrosis (CF) groups

	CF Retrospective group	CF Prospective group	Periportal fibrosis	Irregular liver margins	BDA in the HPB	Contrast media-uptake
ALBI	25 patients 1 8 patients 2	13 patients 1 4 patients 2	$p = 0.37$	$p = 0.11$	$p = 0.47$	$p < 0.005$
CPS	3 patients A 3 patients B	2 patients A	$p < 0.005$	$p < 0.005$	$p < 0.005$	$p = 0.18$

To estimate the severity of liver disease the Albumin-bilirubin (ALBI) score (A1=ALBI score grade 1=early stage, A2=ALBI score grade 2=moderate stage, A3=ALBI score grade 3=advanced stage, not available) and the Child-Pugh Score (CPS) for patients with cirrhosis were applied (A=well compensated cirrhosis, B=moderate functional compromised cirrhosis, C= decompensated cirrhosis, not available)

*p*-values are based upon Pearson chi-square tests

**Table 4** The quantitative values of the cystic fibrosis (CF) groups and controls

Group	CF Retrospective group	CF Prospective group	Controls 1	Controls 2	<i>p</i> -value Retrospective group vs. Controls 1	<i>p</i> -value prospective group vs. controls 2
Patient number	33	17	27	13	n.s.	n.s.
Liver vol. median (cm <sup>3</sup> )	1,025 (805–1,174)	1,047 (921–1,325)	1,194 (823–1,364)	1,023 (724–1,221)	1	0.313
Spleen vol. median (cm <sup>3</sup> )	136 (111–179)	193 (115–259)	87 (60–121)	84 (67–107)	0.0008	0.002
Median portal vein diameter (mm) in post CE pv-images	11 (10–13)	13 (11–15)	11 (10–13)	10 (10–12)	0.887	0.061
RLE (%)	169 (140–197)	187 (130–208)	158 (140–182)	157 (135–197)	0.542	0.392
Liver fat fraction CSI (%)	4 (0–12)	5 (1–13)	1 (1–5)	3 (0–5)	0.138	0.302

Data are presented as median and interquartile range (IQR)

*Vol.* volume, *RLE* relative liver enhancement, *CE* contrast-enhanced, *CSI* chemical shift imaging, *pv* portal venous

*p*-values are based upon Mann-Whitney-U tests

**Qualitative features multivariate analysis**

Among the classification features, the resulting CHAID tree flow chart for the retrospective CF group (Fig. 5) determined three imaging descriptors that had highly statistically significant differences between CFLD patients and controls, namely: (1) the presence of altered gallbladder morphology (GBAM) (Fig. 2); (2) periportal tracking (PPT) seen on DWI (Fig. 3);

and (3) periportal fat deposition (PPFD) seen on T1 chemical shift imaging (Fig. 4). Furthermore, GBAM was the initial splitting predictor, separating those with a high probability of CFLD from the control group (*p*= 0.001).

For the retrospective group, GBAM had a 96% PPV for CFLD. The PPV was 100% in those CF patients who had normal gallbladder morphology but PPT. The NPV was 96% for CFLD in those patients who did not have GBAM,

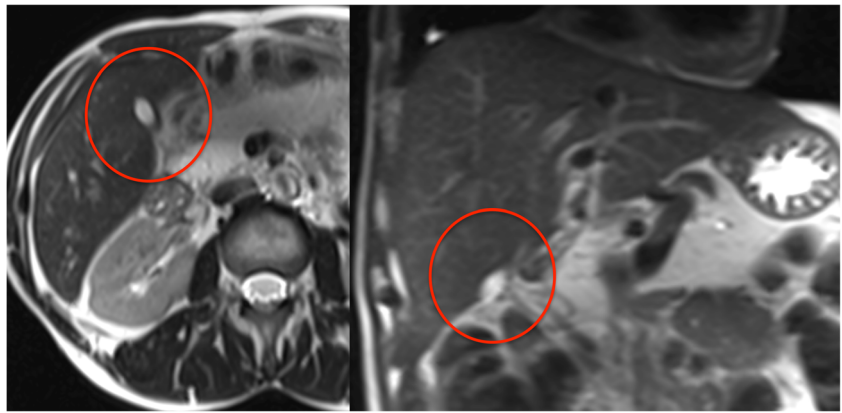
**Table 5** The 15 qualitative features of cystic fibrosis (CF)

	CF Retrospective group	CF Prospective group	Controls 1	Controls 2	<i>p</i> -value Retrospective group vs. controls 1	<i>p</i> -value Prospective group vs. controls 2
Patient number	33	17	27	13	n.s.	n.s.
Diffuse fatty liver changes	9	8	4	4	0.119	0.25
Periportal fat deposition	18	11	4	0	<0.001	<0.001
Periportal tracking DWI	22	12	5	4	<0.001	0.002
Bile duct abnormalities MRCP T2w	12	2	0	0	0.002	0.002
Bile duct abnormalities T1w post CE	14	5	0	0	0.001	<0.001
Heterogeneous liver parenchyma DWI	16	5	0	0	<0.001	<0.001
Heterogeneous liver parenchyma T1w post CE	14	6	0	0	<0.001	<0.001
Degree of hepatobiliary contrast uptake normal	26	14	27	12	0.138	0.45
Timely hepatobiliary excretion	24	15	26	11	0.07	0.095
Gallbladder alterations	24	13	1	2	<0.001	0.013
Periportal fibrosis	10	1	0	0	0.003	0.007
RNH	4	0	0	0	0.075	0.074
Widening of the fissures and hilum	19	4	0	0	<0.001	<0.001
Portal vein diameter Post-CE pv-images >12 mm	11	8	8	3	0.138	0.058
Abnormal lymph nodes in the hepatoduodenal ligament	12	10	9	1	0.053	0.011

*DWI* diffusion-weighted images, *CE* contrast-enhanced, *RNH* regenerative nodular hyperplasia, *pv* portal venous

*p*-values are based upon Pearson chi-square or Fisher’s exact tests as appropriate

**Fig. 2** A 32-year-old male cystic fibrosis (CF) patient: axial and coronal T2-weighted images show an example of altered gallbladder morphology (GBAM), illustrated by a micro-gallbladder. The altered, distinctly shrunken gallbladder is well depicted on the T2-weighted axial and coronal images



PPT or PPF. These three imaging predictors had a sensitivity of 97.0 % (95% CI: 84.2–99.9) and a specificity of 81.5 % (95% CI: 61.9–93.7) for the discrimination of CFLD from controls.

The prospective CF group confirmed the results of the retrospective CF group (Fig. 5). Likewise, GBAM was also the initial splitting predictor in the validation group, according to the CHAID tree flow chart. Fourteen of 17 CF patients had evidence of GBAM, as opposed to two of 13 in the control group ( $p = 0.0001$ ). Two-thirds of CF patients with normal gallbladder morphology showed PPT whereas no control patients did. For the prospective/validation group, the PPV of GBAM for CFLD was 88%. Furthermore, the PPV was 100% if gallbladder morphology was normal but there were signs of PPT. The NPV was 92% for the diagnosis of CFLD if patients did not have GBAM, PPT or PPF. In the validation group, these three imaging predictors had a sensitivity of 94.1 % (95% CI: 71.3–99.9) and a specificity of 84.6 % (95% CI: 54.6–98.1) for the discrimination of CFLD from normal patients.

Furthermore, the area under the ROC curves used to evaluate the diagnostic efficacy in distinguishing CFLD from the controls was 0.96 and 0.90 (Fig. 6) for the test and validation groups, respectively.

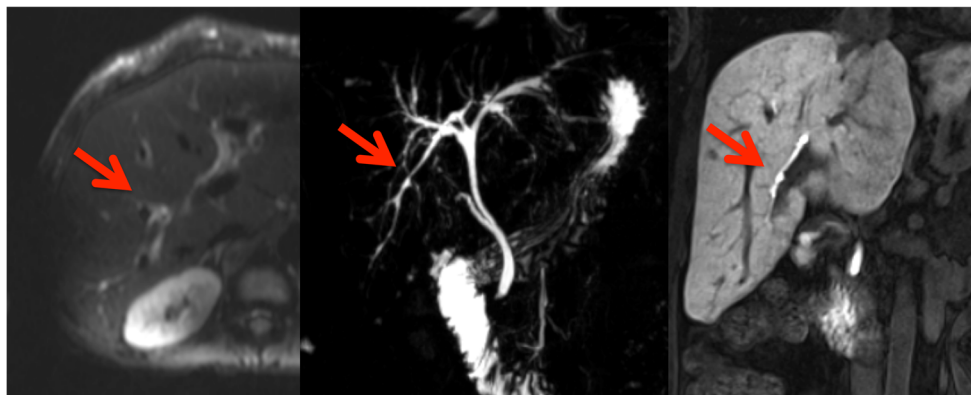


**Fig. 3** In this 25-year-old male cystic fibrosis (CF) patient periportal tracking (PPT) is shown on the diffusion-weighted images, demonstrating a band-like hyperintense signal alteration along the portal triad. Bile duct abnormalities (BDA) are shown in the T2-

## Discussion

Our results obtained from the multivariate (CHAID) analysis showed that the most important and independent MR imaging predictors of CFLD are: (1) the presence of altered gallbladder morphology (GBAM); (2) periportal tracking (PPT) on DWI; and (3) periportal fat deposition (PPFD) on CSI. Using the CHAID statistical method, these three features, i.e. 1–3, also cited in previous studies [26–29], emphasise the fact that CFLD belongs to the group of cholestatic liver diseases [30]. Furthermore, the results from the retrospective cohort were validated by the prospective CF group.

GBAM, as described in the classic cholestatic liver disease PSC, turned out to be the highest-order discriminator between patients with CFLD and controls [32, 33].

In CFLD, the GB alterations have been considered to be due to defects in gallbladder motility and emptying [26, 27, 31]. We assume that CFLD patients have dysfunctional mucosa, which causes these changes either due to increased bile production and decreased biliary hydrophobicity or disrupted enterohepatic circulation of bile acids [31, 32].

The second-order predictors were PPT on DWI and the third PPF on chemical shift imaging, respectively.

weighted magnetic resonance cholangiopancreatography images and in T1-weighted images, in the hepatobiliary phase (20 min after the administration of gadoteric acid) by contour irregularities of the intrahepatic bile ducts

**Fig. 4** A 23-year-old male cystic fibrosis (CF) patient: T1-weighted in- and opposed-phase images demonstrate the periportal fat deposition (PPFD) as a band-like signal intensity loss on the opposed phase image compared to the in-phase image along the fissure of the porta hepatis

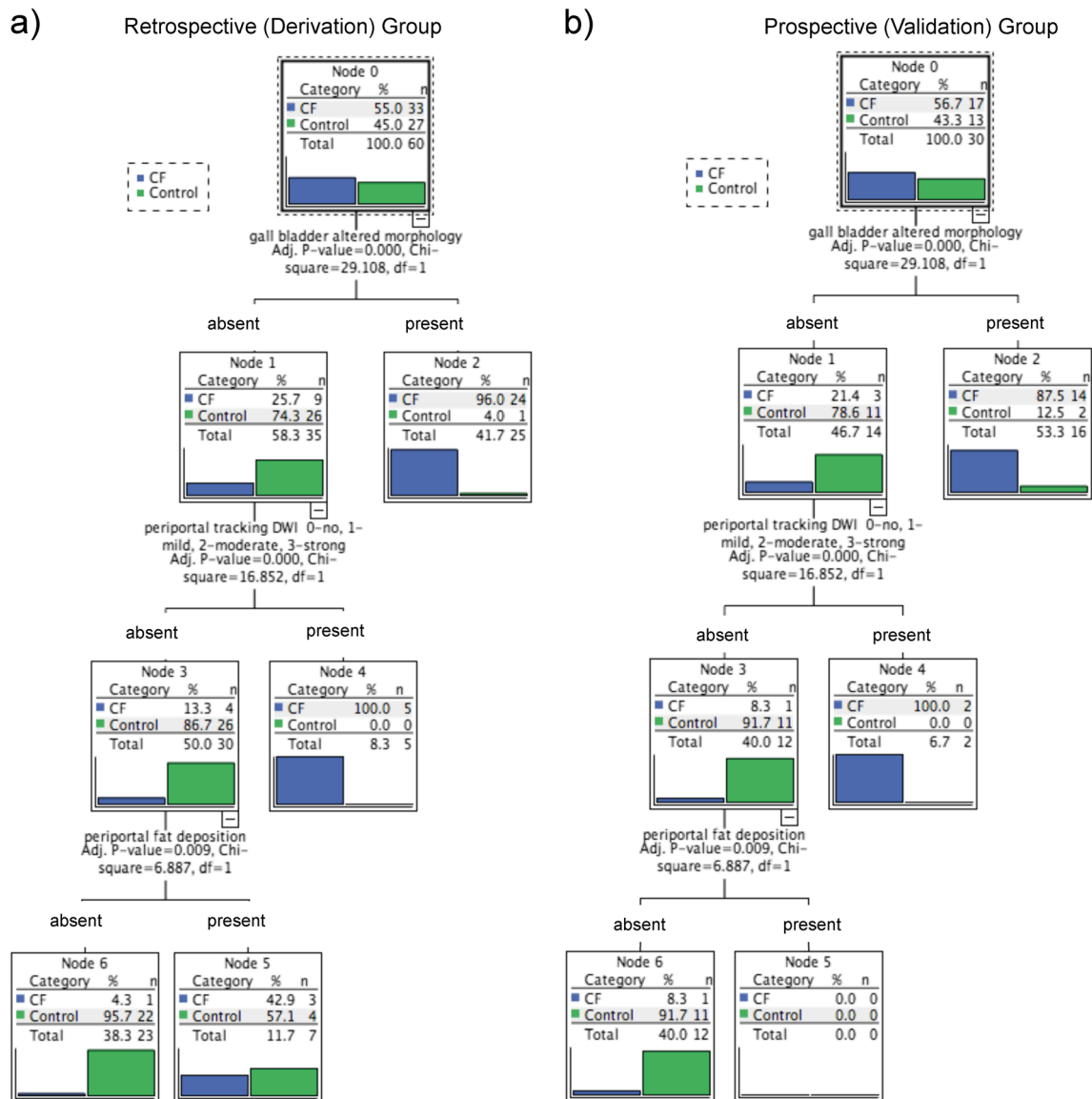
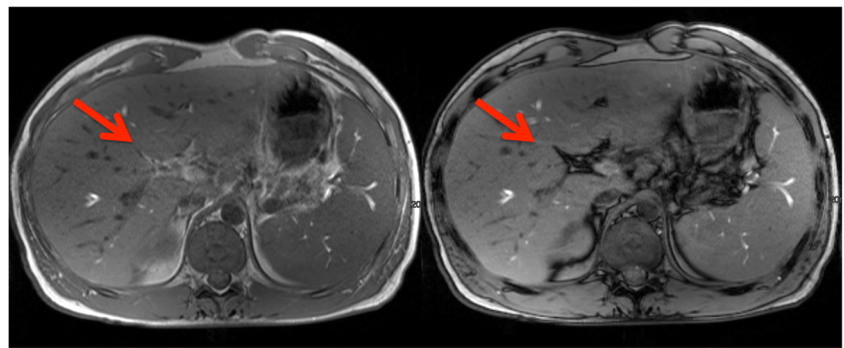
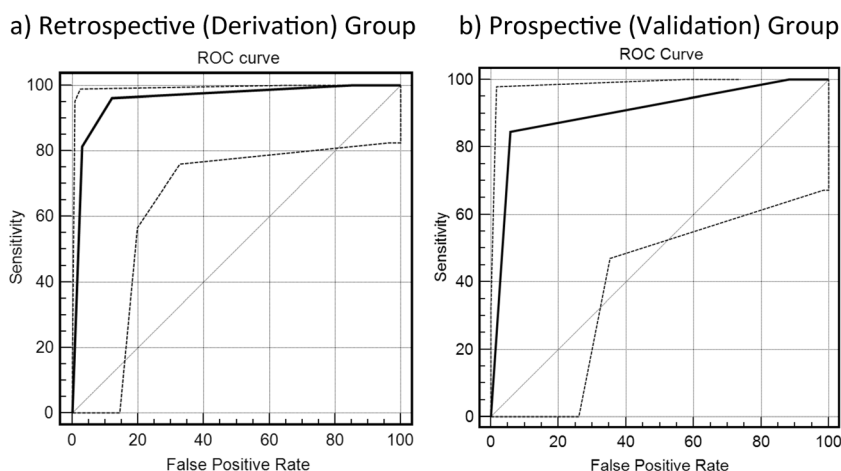


**Fig. 5 (a)** The results, obtained from the multivariate (CHAID-Chi-Squared Automated Interaction Detection Algorithm) analysis for the retrospective cystic fibrosis (CF) group, show three independent MR imaging predictors of cystic fibrosis-associated liver disease (CFLD): the presence of altered gallbladder morphology (GBAM), periportal

tracking (PPT) on diffusion-weighted imaging (DWI), and periportal fat deposition (PPFD) on chemical shift imaging (CSI) in a tree flow chart. **(b)** The tree flow chart for the prospective group confirmed the results obtained from the retrospective group



**Fig. 6** The area under the receiver-operating characteristic (ROC) curve used to evaluate the diagnostic efficacy in distinguishing cystic fibrosis-associated liver disease (CFLD) from the control group is 0.96 for the retrospective cystic fibrosis (CF) group (a) and 0.90 for the prospective/validation CF group (b)



Ductopenia, due to inflammation and oedema along the bile ducts or portal triad, results in wall thickening and fibrosis, which leads to vanishing duct syndrome, a pathognomonic feature of cholestatic liver diseases [33, 34]. Indeed, correlation of US with MR findings showed that periportal echogenicity is more often due to fat rather than fibrosis, as our findings confirmed (i.e. PPF) [35]. Periportal tracking and periportal fat deposition are probably caused by geographic inflammation and oedema along the portal triad, again, characteristic for cholestatic liver diseases. As in PSC, the literature describes a range of intra- and extrahepatic biliary abnormalities for CFLD, including sludge, cholelithiasis, strictures, with or without cholangitis, and periductal fibrosis [36]. Although our results showed a high sensitivity (94.1%), the specificity was rather moderate (84.6%), likely due to the fact that sludge and gallstones are so non-specific, and are also likely to be found in asymptomatic controls. Even by entering the statistically significant laboratory markers from the univariate analysis (ALP and GGT) to the multivariate analysis, there was no incremental value with regard to sensitivity and specificity.

However, in clinical practice, the presence of these imaging features (GBAM, PPT and PPF), in combination with elevated ALP and GGT is extremely rare in healthy patients and highly suggestive of CFLD in CF patients.

Furthermore, these imaging features correlated well with ALP and GGT levels ( $p < 0.05$ ) but not with the ALT and AST levels ( $p > 0.05$ ), again underlining the cholestatic nature of CFLD. The lack of correlation of imaging findings with serum bilirubin levels ( $p > 0.05$ ) is not surprising as bilirubin levels rise late in cholestatic liver diseases. This is, again, our explanation for the dissociation between the quantitative parameters, including liver volume, portal vein diameter and RLE. As for bilirubin, we would expect an increase in portal diameter or a decrease in RLE and liver volume only in very advanced CFLD. In early disease, the liver can still compensate. On the contrary, the splenic volume was the sole quantitative

parameter that demonstrated significance ( $p < 0.05$ ) [37]. We attribute this to either inflammatory/immunological changes or incipient, rather than significant, portal hypertension.

Although steatosis has been reported in up to 60% of CF patients [29] and is included in the Debray classification as one of the diagnostic criteria of CFLD, we found no significant hepatic fat fraction measured on CSI ( $p = 0.30$ ). This was expected, as there has been no proven relationship between steatosis and CFLD. When present, steatosis is likely a concomitant finding, either due to diabetes or medications [38]. Similarly, according to our results, hepatomegaly was not confirmed as a criterion of CFLD, which was not surprising since hepatomegaly as judged by clinical examination is known to be imprecise.

In general, CFLD is felt to be an emerging entity, Koh C. et al recently emphasized [39] the lack of sufficient characterisation and diagnostic tools for the diagnosis of adult-onset CFLD. They found that only 22% of CF patients had CFLD, based upon the Debray criteria, which they felt was likely an underestimation of actual disease.

Beyond finding an excellent sensitivity of MRCP [40] for depicting CFLD, we observed that none of the three imaging features (i.e. GBAM, PPT and PPF) required CM administration for detection. However, gadoxetic acid-enhanced MRI simply improved detection of bile duct abnormalities and allowed us to evaluate liver function impairment based upon liver parenchymal enhancement in the hepatobiliary phase, i.e. 20 min after the injection of CM [41, 42].

The ALBI score associated well with the biomarkers of liver function derived from the uni- and multivariate analyses with regard to the severity of the disease, whereas the Child-Pugh score was associated only with the morphological changes including periportal fibrosis, bile duct abnormalities and liver contour irregularity, but not with contrast media uptake in the hepatobiliary phase. This is in keeping with the subjective nature of the CPS. The presence of altered liver morphology and decreased uptake of CM in the HBP were

found in patients with more advanced disease, i.e. CPS B or ALBI grade 2. These findings can be explained by the fact that the ALBI score seems to be more sensitive in estimating disease severity than CPS, a fact already recognized in the literature [43, 44].

Our study's limitations include, firstly, the retrospective nature of the majority of the cohort with the inherent limitations of a retrospective study. However, the results derived from this retrospective group were confirmed in the prospective group, which validated the applicability of the established classification algorithm. Another potential bias is that most of the patients had undergone lung transplantation and were therefore on immunosuppressants and other drugs, which are potential confounders of liver function results. However, our results were well in line with other clinical publications [7]. Furthermore, although our cohorts were not subject to histopathology staging, clinical, laboratory and MR features strongly suggest that the majority had early-stage CFLD. The lack of elevated serum bilirubin, as well as the absence of impaired uptake or excretion on hepatobiliary imaging support this conclusion [45].

There is no gold standard for CFLD diagnosis; even the universally-accepted Debray criteria, which may appear simpler and cheaper than liver MRI, is based largely on clinical signs, laboratory tests and ultrasound. Therefore, we feel that the integration of MRI in CFLD screening and follow-up might improve diagnosis of CFLD, when laboratory tests and/or clinical signs fail to do so.

In conclusion, a short unenhanced MRI protocol can identify the three cardinal imaging features of CFLD, namely altered gallbladder morphology, periportal tracking and periportal fat deposition. The hepatobiliary phase of gadoteric acid-enhanced MRI can define the progression of CFLD.

**Acknowledgements** Open access funding provided by Medical University of Vienna.

**Funding** Only one of the authors has received funding (supported by funds of the Austrian National Bank/Oesterreichische Nationalbank, Anniversary Fund, project number: AP15711ONB). The remaining authors have not received any funding.

## Compliance with ethical standards

**Guarantor** The scientific guarantor of this publication is Ahmed Ba-Ssalamah.

**Conflict of interest** Ahmed Ba-Ssalamah received honoraria for lectures and consultancy from Bayer but disclosed no relation to the present article.

The other authors of this manuscript declare no relationships with any companies whose products or services may be related to the subject matter of the article.

**Statistics and biometry** Michael Weber kindly provided statistical advice for this manuscript.

Additionally, one of the authors has significant statistical expertise (Pascal Baltzer).

**Informed consent** Written informed consent was waived by the Institutional Review Board.

**Ethical approval** Institutional Review Board approval was obtained.

## Methodology

- Prospective/retrospective
- Observational study
- Performed at one institution

**Open Access** This article is distributed under the terms of the Creative Commons Attribution 4.0 International License (<http://creativecommons.org/licenses/by/4.0/>), which permits unrestricted use, distribution, and reproduction in any medium, provided you give appropriate credit to the original author(s) and the source, provide a link to the Creative Commons license, and indicate if changes were made.

## References

1. Stoltz DA, Meyerholz DK, Welsh MJ (2015) Origins of cystic fibrosis lung disease. *N Engl J Med* 372:1574–1575
2. Harring TR, Nguyen NT, Liu H, Karpen SJ, Goss JA, O'Mahony CA (2013) Liver transplantation in cystic fibrosis: a report from Baylor College of Medicine and the Texas Children's Hospital. *Pediatr Transplant* 17:271–277
3. Chrysostalis A, Hubert D, Coste J et al (2011) Liver disease in adult patients with cystic fibrosis: a frequent and independent prognostic factor associated with death or lung transplantation. *J Hepatol* 55:1377–1382
4. Leeuwen L, Fitzgerald DA, Gaskin KJ (2014) Liver disease in cystic fibrosis. *Paediatr Respir Rev* 15:69–74
5. Parisi GF, Di Dio G, Franzonello C et al (2013) Liver disease in cystic fibrosis: an update. *Hepat Mon* 13:e11215
6. Nash EF, Völling C, Gutierrez CA et al (2012) Outcomes of patients with cystic fibrosis undergoing liver transplantation with and without cystic fibrosis-associated liver cirrhosis. *Clin Transplant* 26:34–41
7. Staufer K, Halilbasic E, Trauner M, Kazemi-Shirazi L (2014) Cystic fibrosis related liver disease—another black box in hepatology. *Int J Mol Sci* 15:13529–13549
8. Bhardwaj S, Canlas K, Kahi C et al (2009) Hepatobiliary abnormalities and disease in cystic fibrosis: epidemiology and outcomes through adulthood. *J Clin Gastroenterol* 43:858–864
9. Kobelska-Dubiel N, Klineciewicz B, Cichy W (2014) Liver disease in cystic fibrosis. *Prz Gastroenterol* 9:136–141
10. Stonebraker JR, Ooi CY, Pace RG et al (2016) Features of Severe Liver Disease With Portal Hypertension in Patients with Cystic Fibrosis. *Clin Gastroenterol Hepatol*. <https://doi.org/10.1016/j.cgh.2016.03.041>
11. Lewindon PJ, Pereira TN, Hoskins AC et al (2002) The role of hepatic stellate cells and transforming growth factor-beta(1) in cystic fibrosis liver disease. *Am J Pathol* 160:1705–1715
12. Asayama Y, Nishie A, Ishigami K et al (2016) Heterogeneity of non-cancerous liver parenchyma on gadoteric acid-enhanced MRI: an imaging biomarker for hepatocellular carcinoma development in chronic liver disease. *Clin Radiol* 71:432–437
13. Nakayama T, Yoshiura T, Nishie A et al (2016) Balanced MR cholangiopancreatography with motion-sensitized driven-equilibrium (MSDE) preparation: feasibility of Gd-EOB-DTPA-enhanced biliary examination. *Clin Radiol*. <https://doi.org/10.1016/j.crad.2016.03.019>
14. Lee NK, Kim S, Kim DU et al (2015) Diffusion-weighted magnetic resonance imaging for non-neoplastic conditions in the

- hepatobiliary and pancreatic regions: pearls and potential pitfalls in imaging interpretation. *Abdom Imaging* 40:643–662
15. Debray D, Kelly D, Houwen R, Strandvik B, Colombo C (2011) Best practice guidance for the diagnosis and management of cystic fibrosis-associated liver disease. *J Cyst Fibros* 10(Suppl 2):S29–S36
  16. Boyle MP (2003) Nonclassic cystic fibrosis and CFTR-related diseases. *Curr Opin Pulm Med* 9:498–503
  17. Pugh RN, Murray-Lyon IM, Dawson JL, Pietroni MC, Williams R (1973) Transection of the oesophagus for bleeding oesophageal varices. *Br J Surg* 60:646–649
  18. Johnson PJ, Berhane S, Kagebayashi C et al (2015) Assessment of liver function in patients with hepatocellular carcinoma: a new evidence-based approach—the ALBI grade. *J Clin Oncol* 33:550–558
  19. Muggli D, Muller MA, Karlo C, Fornaro J, Marincek B, Frauenfelder T (2009) A simple method to approximate liver size on cross-sectional images using living liver models. *Clin Radiol* 64:682–689
  20. Lemaitre C, Dominique S, Billoud E et al (2016) Relevance of 3D Cholangiography and Transient Elastography to Assess Cystic Fibrosis-Associated Liver Disease? *Can Respir J* 2016:4592702
  21. Koelblinger C, Krssak M, Maresch J et al (2012) Hepatic steatosis assessment with 1H-spectroscopy and chemical shift imaging at 3.0 T before hepatic surgery: reliable enough for making clinical decisions? *Eur J Radiol* 81:2990–2995
  22. Tran VT, Vasanawala S (2013) Pediatric hepatobiliary magnetic resonance imaging. *Radiol Clin North Am* 51:599–614
  23. Van Beers BE, Daire JL, Garteiser P (2015) New imaging techniques for liver diseases. *J Hepatol* 62:690–700
  24. Gupta AA, Kim DC, Krinsky GA, Lee VS (2004) CT and MRI of cirrhosis and its mimics. *AJR Am J Roentgenol* 183:1595–1601
  25. Baltzer PA, Dietzel M, Kaiser WA (2013) A simple and robust classification tree for differentiation between benign and malignant lesions in MR-mammography. *Eur Radiol* 23:2051–2060
  26. Jebbink MC, Heijerman HG, Masclee AA, Lamers CB (1992) Gallbladder disease in cystic fibrosis. *Neth J Med* 41:123–126
  27. Curry MP, Hegarty JE (2005) The gallbladder and biliary tract in cystic fibrosis. *Curr Gastroenterol Rep* 7:147–153
  28. Durieu I, Pellet O, Simonot L et al (1999) Sclerosing cholangitis in adults with cystic fibrosis: a magnetic resonance cholangiographic prospective study. *J Hepatol* 30:1052–1056
  29. Lavelle LP, McEvoy SH, Ni Mhurchu E et al (2015) Cystic Fibrosis below the Diaphragm: Abdominal Findings in Adult Patients. *Radiographics* 35:680–695
  30. Robertson MB, Choe KA, Joseph PM (2006) Review of the abdominal manifestations of cystic fibrosis in the adult patient. *Radiographics* 26:679–690
  31. Debray D, Rainteau D, Barbu V et al (2012) Defects in gallbladder emptying and bile Acid homeostasis in mice with cystic fibrosis transmembrane conductance regulator deficiencies. *Gastroenterology* 142(1581-1591):e1586
  32. Bodewes FA, van der Wulp MY, Beharry S et al (2015) Altered intestinal bile salt biotransformation in a cystic fibrosis (Cfr-/-) mouse model with hepato-biliary pathology. *J Cyst Fibros* 14:440–446
  33. Desmet VJ (1998) Histopathology of chronic cholestasis and adult ductopenic syndrome. *Clin Liver Dis* 2:249–264 viii
  34. Burt AD (2002) Primary biliary cirrhosis and other ductopenic diseases. *Clin Liver Dis* 6(363-380):vi
  35. King LJ, Scurr ED, Murugan N, Williams SG, Westaby D, Healy JC (2000) Hepatobiliary and pancreatic manifestations of cystic fibrosis: MR imaging appearances. *Radiographics* 20:767–777
  36. Ruiz A, Lemoine S, Carrat F, Corpechot C, Chazouilleres O, Arrive L (2014) Radiologic course of primary sclerosing cholangitis: assessment by three-dimensional magnetic resonance cholangiography and predictive features of progression. *Hepatology* 59:242–250
  37. Van Biervliet S, Robberecht E (2007) Splenectomy in cystic fibrosis. *Arch Dis Child* 92:277–278
  38. Fotbolcu H, Zorlu E (2016) Nonalcoholic fatty liver disease as a multi-systemic disease. *World J Gastroenterol* 22:4079–4090
  39. Koh C, Sakiani S, Surana P et al (2017) Adult-onset cystic fibrosis liver disease: Diagnosis and characterization of an underappreciated entity. *Hepatology* 66:591–601
  40. Yam BL, Siegelman ES (2014) MR imaging of the biliary system. *Radiol Clin North Am* 52:725–755
  41. Wibmer A, Nolz R, Trauner M, Ba-Ssalamah A (2015) Functional MR imaging of the liver. *Radiologe* 55:1057–1066
  42. Neri E, Bali MA, Ba-Ssalamah A et al (2016) ESGAR consensus statement on liver MR imaging and clinical use of liver-specific contrast agents. *Eur Radiol* 26:921–931
  43. Zou H, Yang X, Li QL, Zhou QX, Xiong L, Wen Y (2018) A Comparative Study of Albumin-Bilirubin Score with Child-Pugh Score, Model for End-Stage Liver Disease Score and Indocyanine Green R15 in Predicting Posthepatectomy Liver Failure for Hepatocellular Carcinoma Patients. *Dig Dis* 36:236–243
  44. Cui E, Long W, Luo L, Hu M, Huang L, Chen X (2017) Development and validation of a predictor of insufficient enhancement during the hepatobiliary phase of Gd-EOB-DTPA-enhanced magnetic resonance imaging. *Acta Radiol* 58:1174–1181
  45. Tschirch FT, Struwe A, Petrowsky H, Kakales I, Marincek B, Weishaupt D (2008) Contrast-enhanced MR cholangiography with Gd-EOB-DTPA in patients with liver cirrhosis: visualization of the biliary ducts in comparison with patients with normal liver parenchyma. *Eur Radiol* 18:1577–1586